MIT Open Access Articles

Coordination number model to quantify
packing morphology of aligned nanowire arrays

Massachusetts Institute of Technology

Coordination Number Model to Quantify Packing Morphology of Aligned Nanowire Arrays[†]

Itai Y. Stein,[*a§] **and Brian L. Wardle**[b§]

The average inter-wire spacing in aligned nanowire systems strongly influences both the physical and transport properties of the bulk material. Because most studies assume that the nanowire coordination is constant, a model that provides an analytical relationship between the average inter-wire spacings and measurable physical properties, such as nanowire volume fraction, is necessary. Here we report a continuous coordination number model with an analytical relationship between the average nanowire coordination, diameter, and volume fraction. The model is applied to vertically aligned carbon nanotube (VACNT) and nanofiber (VACNF) arrays, and the effective nanowire coordination number is established from easily accessible measures, such as the nanowire spacing and diameter. VACNT analysis shows that the coordination number increases with increasing nanowire volume fraction, leading the measured inter-CNT spacing values to deviate by as much as 13% from the spacing values predicted by the typically assumed hexagonal packing. VACNF analysis suggests that, by predicting an inter-fiber spacing that is within 6% of the reported value, the continuous coordination model outperforms both square and hexagonal packing in real nanowire arrays. Using this model, the average inter-wire spacing of nanowire arrays can be predicted, thus allowing more precise morphology descriptions, and thereby supporting the development of more accurate structure-property models of bulk materials comprised of aligned nanowires.

1   Introduction

The exceptional electrical,[1–4] thermal,[5,6] and mechanical properties[7–9] of nanowires have prompted their development for use in high value macroscopic structures such as microprocessors,[10] medical devices,[11,12] energy storage devices,[13] and nanowire array composites.[14] Due to the strong influence of nanowire proximity effects on the mechanical, thermal, electrical, and mass transport properties of macroscopic structures composed of aligned nanowires, the inter-wire spacing, a function of the nanowire coordination number, is very important. But in most cases, the nanowire coordination number is either assumed[15,16] or neglected[16,17] altogether. This stems from the lack of an accessible theoretical model that can quantify the average spacing of nanowires with a diameter in the single nanometer length scale, where the minimum allowable spacing is on the order of a few angstroms. In principle, existing models for random packing of circles in a plane for millimeter length scale systems[18–20] can be extended to the nano scale, thereby allowing the extraction of the average inter-wire spacing through the def-

inition of two dimensional nanowire lattices, and the subsequent calculation of the average two dimensional nanowire nearest neighbor coordination number. Here we report a method for extracting the average coordination number and inter-wire spacing of nanowires in aligned nanowire arrays of varying volume fraction. We find that the average coordination number of the nanowires is not constant, and varies with the nanowire volume fraction.

The development of a continuous model for the average inter-wire spacing of nanowires in a nanowire array was possible through the application of the theoretical model to exemplary systems of nanowires, which included Carbon Nanotubes (CNTs), and Carbon Nanofibers (CNFs). Due to their phenomenal physical[21–23] and transport[24–29] properties, as well as their well-documented use in macroscopic materials, both in forest[15,16,30–34] and nanocomposite[16,17,35–37] forms, arrays of vertically aligned CNTs (VACNTs) were selected to act as the reference system for the continuous coordination model. Arrays of bamboo-like vertically aligned CNFs (VACNFs) are studied to demonstrate how the model can be applied to predict the average spacing of virtually any aligned nanowire system, using well-documented measures of morphology,[38–42] and to compare to a previously reported average inter-fiber spacing study.[42]
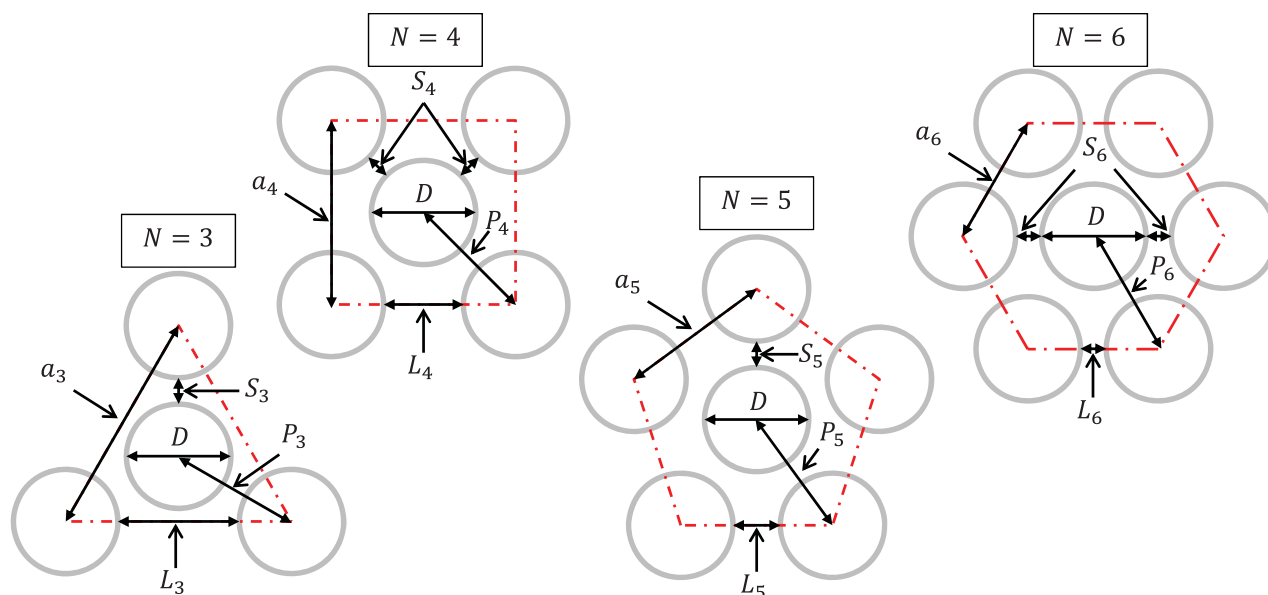
Since nanowire arrays are inherently wavy, the effect of nanowire waviness on the predicted average inter-wire spacing is discussed, and a method for waviness correction is presented. By applying this continuous coordination model to nanowire systems, more precise morphology quantification of nanowire arrays is possible, which could lead to better material property

Fig. 1 Unit cells of the four different coordinations used to model the morphology of nanowire arrays comprised of nanowires of diameter D. The unit cell inter-wire spacing, S_N, and the lattice constant inter-wire spacing, L_N, are both indicated.

prediction for macroscopic architectures composed of aligned nanowires. Using this knowledge, better materials solutions for aerospace, energy, microelectronic, and healthcare applications can be designed and manufactured.

2 Model Development

2.1 Coordination Number Relations

To assess the nearest coordination of the underlying nanowires, the following unit cells as a function of the two dimensional nanowire coordination number (N) are defined (see Fig. 1 for their illustration): triangular ($N = 3$), square ($N = 4$), pentagonal ($N = 5$), and hexagonal ($N = 6$). Since the triangular coordination corresponds to hexagonal coordination with missing nanowires (vacancies), to avoid the accidental definition of hexagonal coordination, the triangular coordination must be limited to a scarce number of unit cells, and is therefore only justified at low nanowire volume fractions.

Using these coordinations, the underlying triangles that make up each unit cell in Fig. 1 can be defined (see Fig. S1 in the ESI† for details). These constitutive triangles are important because they can be packed to form both complete and incomplete (inter-penetrating) arrays of different unit cells, while still remaining within the theoretical framework defined in this report. This is a more realistic approximation of amorphous materials than simply tiling the full unit cells presented in Fig. 1. Also, using these constitutive triangles, the maximum volume fraction for each lattice can be calculated. The volume fraction (V_f) and theoretical maximum volume fraction (V_f^{max}) for each coordination can be calculated using the following equations:

$$V_{f,\,N}(D, P_N) = \frac{\pi D^2}{8A_{\triangle,\,N}(P_N)} \quad (1)$$

$$V_{f,\,N}^{max}(D = P_N) = \frac{\pi P_N^2}{8A_{\triangle,\,N}(P_N)} \quad (2)$$

Where $A_{\triangle}$ is the area of the triangle, D is the diameter of the nanowires, $P_N = D + S_N$ where S_N is the unit cell inter-wire spacing, and N is the coordination number. See Table S1 in the ESI† for the expanded forms of $A_{\triangle,\,N}(P_N)$, and $V_{f,\,N}(D, P_N)$ for each coordination. S_N, and the lattice constant spacing, defined as L_N, are also shown in Fig. 1.

Next the inter-wire spacing, S_N is calculated for each coordination. To do so, Eq. 1 is solved for S_N, and the result is substituted into Eq. 2 yielding the following equation for S_N:

$$S_N = D\left(\sqrt{\frac{V_{f,\,N}^{max}}{V_f}} - 1\right) \quad (3)$$

The lattice constant spacing, L_N, must also be considered before the average inter-wire spacing for each coordination can be derived. Using the constitutive triangles for each coordination, shown in Fig. S1 in the ESI,† lattice constants, defined as a_N, for each coordination can be calculated as a function of D taking the following form:

$$a_N(D, V_f) = \chi_N D\left(\sqrt{\frac{V_{f,\,N}^{max}}{V_f}}\right) \quad (4)$$

Where χ_N is 1 for hexagonal and > 1 for the other coordinations. $a_N(D, V_f)$ and χ_N for each coordination are shown in Table S2 in the ESI.†

Next, L_N is calculated, and takes the following form:

$$L_N(D,V_f) = D\left(\chi_N\left(\sqrt{\frac{V_{f,N}^{max}}{V_f}}\right)-1\right) \quad (5)$$

Defining the average inter-wire spacing, Γ_N, as the average a_N and L_N yields:

$$\Gamma_N(D,V_f) = D\left(\left(\frac{\chi_N+1}{2}\right)\left(\sqrt{\frac{V_{f,N}^{max}}{V_f}}\right)-1\right) \quad (6)$$

The full form of $\Gamma_N(D,V_f)$ for each coordination is shown in Table S2 of the ESI.†

One of the purposes of this model is to quantify a nanowire array's deviation from that of an ideally (hexagonally) packed nanowire array. To illustrate this deviation, all average spacing equations are re-written as a function of the theoretical maximum volume fraction for hexagonal close packing in two dimensions, $V_{f,6}^{max} = 90.69\%$. $V_{f,6}^{max}$ should not be confused with the maximum volume fraction for hexagonal close packing of monodisperse spheres in three dimensions, $V_{f,6}^{max}(spheres) = \frac{\pi}{\sqrt{18}} \approx 74.05\%$, which was proven by C.F. Gauss to have the highest packing density of any spherical lattice in three dimensions[43]. The simplified Γ_N functions take the general form of:

$$\Gamma_N(D,V_f) = D\left(\delta_N\left(\sqrt{\frac{0.9069}{V_f}}\right)-1\right) \quad (7)$$

Where δ_N is interpreted as a deviation factor from the ideal (hexagonal) nanowire packing that has the following values:

$$\delta_N = \begin{cases} 1, & N = 6 \\ > 1, & 3 \leq N < 6 \end{cases}$$

The exact values of δ_N for each coordination can be found in Table S3 in the ESI.†

To turn this series of discrete values into a continuous function of N, the values of the δ_N were plotted and fitted with a power function of the following form:

$$\delta_N = a_1(N)^{b_1} + c_1 \quad (8)$$

Where the fitting coefficients are ($R^2 = 0.9999$): $a_1 = 11.77$, $b_1 = -3.042$, $c_1 = 0.9496$. A plot of the values of δ_N and the fitting can be found in Fig. S2 in the ESI.†, and the expanded form of the average inter-wire spacing using Eq. 8 can be found in Eq. S1 in the ESI.† By using Eq. S1 from the ESI,† a continuous coordination number as a function of average spacing, volume fraction, and nanowire diameter can be defined:

$$N(D,\Gamma_N,V_f) = \left(\frac{\frac{\Gamma_N}{D}+1}{11.77\sqrt{\frac{0.9069}{V_f}}} - \frac{0.9496}{11.77}\right)^{-\frac{1}{3.042}} \quad (9)$$

Using this equation for the coordination number, experimentally determined values for the average spacing, nanowire diameter, and volume fraction can be used to calculate a relationship between the coordination number and the volume fraction, thereby allowing the definition of an equation for the average spacing that is only a function of volume fraction and nanowire diameter, both of which are relatively simple to determine experimentally.

2.2 Application to Real Aligned Nanowire Arrays

To apply this model to real aligned nanowire arrays, the physically limited minimum inter-wire spacing must be considered. For Carbon nanowires (such as CNTs and CNFs), graphitic spacing of 0.34 nm[15] can be used as the real lower bound on the spacing, S^{LB}, in the nanowire array. By using the nanowire diameter, D, the real upper bound of the volume fraction (V_f^{UB}) for each coordination can be evaluated. Using hexagonal coordination ($N = 6$ from Eq. 2), V_f^{UB} for any aligned nanowire system can be calculated as follows:

$$V_f^{UB}(D,S^{LB}) = \frac{\sqrt{3}\pi}{6}\left(\frac{D}{D+S^{LB}}\right)^2 \quad (10)$$

The resulting V_f^{UB} values for the 8 nm diameter CNTs used in this report is 83.45 volume %. To apply this model to non-carbon based nanowire arrays, a different S^{LB} would need to be selected, resulting in different V_f^{UB} values for nanowire arrays of the same diameter but different composition.

3 Experimental

Here we use the results of the continuous coordination model to investigate the average coordination of a system of nanowires composed of synthesized in-house, 8 nm diameter VACNTs.

3.1 Aligned CNT Array Synthesis

Aligned multiwalled CNT (MWCNT) forests were grown in a 22 mm internal diameter quartz tube furnace at atmospheric pressure via a previously described thermal catalytic chemical vapor deposition (CVD) process using ethylene as the carbon source.[17,35–37] CNT growth takes place at a nominal temperature of $750°C$, with an average growth rate of $\sim 2 \frac{\mu m}{s}$.[17,35] CNT arrays were grown on 1×1 cm^2 Si substrates with a catalytic layer composed of 1 nm Fe/10 nm Al_2O_3 deposited by electron beam deposition, forming vertically aligned, 1.0 volume % dense, 8 nm diameter, millimeter length scale MWCNT arrays.[17,35,36] As grown (1.0 volume %) CNT forests are then delaminated from the Si substrate using a standard lab razor blade, and densified using biaxial mechanical densification to the desired CNT volume fraction (up to 20.0 volume %)[16].
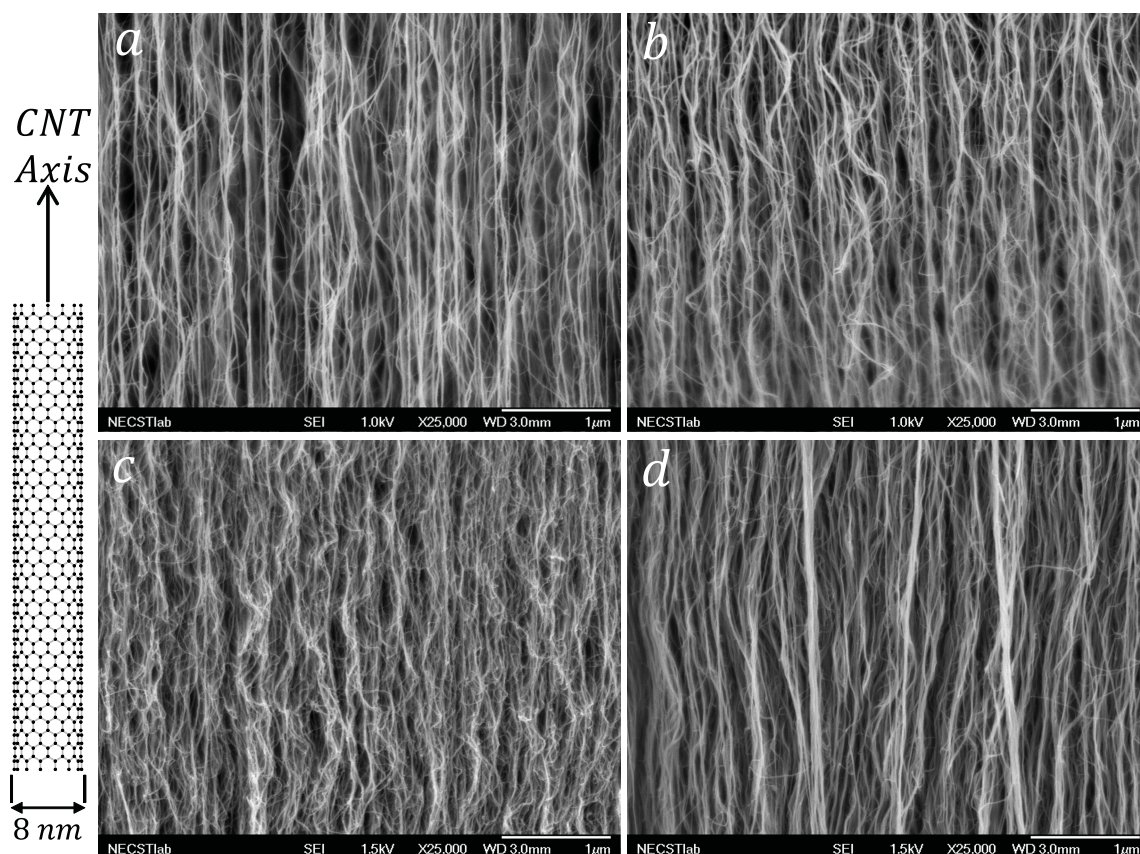
Fig. 2 HRSEM micrographs of (a) 1.0 volume %; (b) 6.0 volume %; (c) 10.6 volume %; (d) 20.0 volume % CNT forests. The waviness of the CNTs can be seen quite clearly in the lower volume fraction arrays (a and b), but is less distinct in the higher volume fraction arrays (c and d).

### 3.2 High Resolution Scanning Electron Microscopy and Image Analysis

To generate representative micrographs of the surface morphology of the CNT forests, HRSEM analysis was performed using a JEOL 6700 cold field-emission gun scanning electron microscope (FEGSEM) using secondary electron imaging (SEI) at an accelerating voltage ranging from 1.0 to 1.5 kV with a working distance of 3.0 *mm*. CNT forests were imaged in the middle of the sample cross-section to avoid the edge effects that result from the delamination (on the bottom) and growth termination (on the top) of the CNT forests.

To determine the average spacing of the CNTs, lines were drawn perpendicular to the alignment of the CNT on HRSEM micrographs, and the number of CNTs per unit of line length was approximated by using the following algorithms tailored to forests of varying CNT volume fractions: for 1.0 and 6.0 volume % forests only the bright in-focus CNTs were counted as 1, and other CNTs were neglected; for 10.6 and 20.0 volume % forests, all individually distinguished CNTs were counted, and bright bundles of CNTs were counted as 2 CNTs. While this methodology is less rigorous than that found elsewhere[44,45] and could potentially lead to over or underestimation, it is sufficient to demonstrate the use of the theoretical spacing model,

and illustrates the difficulty of using imaging to empirically determine the average spacing in such a system. Also, because HRSEM images of the CNT forests are projections of a three dimensional system onto a plane, a correction factor for the depth lost in the projection process is necessary. To derive the correction factor, the escape depth of secondary electrons, defined as the depth above which no secondary electron can escape the material, must be considered. Typical escape depths of secondary electrons are on the order of $1 - 10$ *nm*, where 1 *nm* is a reasonable order of magnitude for the escape depth of secondary electrons in conducting materials.[46] To calculate the corrected average inter-CNT spacings (Γ_N) and N, the average inter-CNT spacings calculated from the HRSEM images, Γ^{SEM}, was corrected using a 1 *nm* secondary electron escape depth, ℓ_e^{SE}. See Eq. S2 in the ESI† for details. A selection of the HRSEM micrographs used in the average spacing analysis can be found in Fig. 2.

4 Results and Discussion

Here we use the experimentally determined average inter-CNT spacing calculated from HRSEM micrographs (see Fig. S3 in the ESI† for a worked example of how HRSEM micrographs
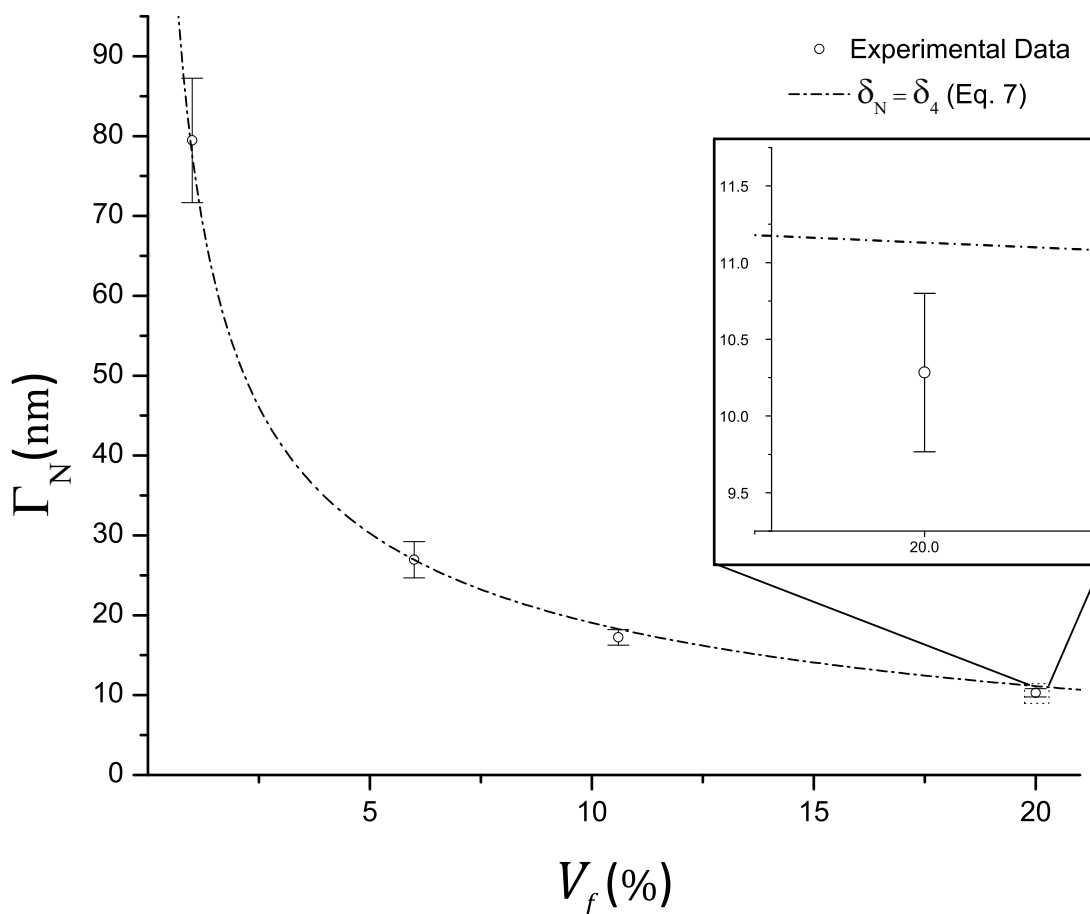
Fig. 3 Average inter-CNT spacing vs. CNT volume fraction with error bars illustrating the standard deviations. The data point at 20.0 volume % is enlarged to clarify the disagreement between the experimental data and the square packing model ($\delta_N = \delta_4$). The data takes a form similar to $D_{CNT}\left(\delta_N\left(\sqrt{\frac{0.9069}{V_f}}\right)-1\right)$ as predicted by the model (Eq. 7).

were used to determine the average inter-CNT spacing in Fig. 3) to examine the effect of varying CNT volume fractions on the coordination number of the system. The continuous coordination model is then applied to a VACNF system, and its predictions are compared to common constant coordination models, namely square ($N = 4$) and hexagonal ($N = 6$) packing. Finally, the influence of nanowire waviness on the model, and a way for its inclusion in the future, are presented.

4.1 VACNT Experimental Results

Average inter-CNT spacing data for samples with CNT volume fractions ranging from 1.0 to 20.0 volume % were calculated from 25 HRSEM micrographs, and corrected for the loss of three dimensional depth information using Eq. S2 from the ESI.† A plot of the average inter-CNT spacing can be found in Fig. 3. At 1.0 volume % CNTs, the value of Γ_N is 79.47 ± 7.79 *nm*, resulting in a *N* value of 3.83, illustrating that square packing would likely underpredict the average inter-CNT spacing at low CNT volume fractions. Samples with 6.0 volume

% CNT yielded a Γ_N value of 26.95 ± 2.26 *nm*, which result in a *N* value of 4.00, thereby indicating that the coordination number of the CNT array increases as a function of CNT volume fraction, and that square packing might be appropriate for CNT volume fractions around 5 volume %. With Γ_N and *N* values of 17.24 ± 0.97 *nm* and 4.41, and 10.28 ± 0.52 *nm* and 4.47, samples with CNT volume fractions of 10.6 and 20.0 volume % continue to demonstrate that the two dimensional nanowire coordination number increases as a function of CNT volume fraction, though not necessarily in a linear fashion, and that the as-

Table 1 Measured and corrected average inter-CNT spacing, and coordination numbers for all CNT volume fractions.

$V_f(\%)$	$\Gamma_N^{SEM}(nm)$	$\Gamma_N(nm)$	N
1.0	79.58 ± 8.15	79.47 ± 7.79	3.83
6.0	26.89 ± 2.38	26.95 ± 2.26	4.00
10.6	17.15 ± 1.01	17.24 ± 0.97	4.41
20.0	10.23 ± 0.52	10.28 ± 0.52	4.47

sumption of constant coordination is only approximate. Γ_N, N, and the experimentally determined Γ_N^{SEM} values can be found in Table 1.

In their paper, T.I. Quickenden and G.K. Tan reported that the coordination number of a system of uniform millimeter length scale disks, defined as the number of disks that made contact with a central disk, increased in an approximately linear fashion from a disk packing fraction of 10 volume % up to a packing fraction of 83 volume %.[19] Beyond 83 volume %, the coordination number of the system was observed to increase in a non-linear fashion until reaching, and plateauing, at a coordination number value of 6.0.[19] Since V_f^{UB} of the CNTs in the array is 83.4 volume % CNTs, the shape of the fit applied to the data should be approximately linear from $V_f = 10$ volume % CNTs up to $V_f = 20$ volume % CNTs, and should remain linear until a much higher V_f. Since previously reported data at $V_f < 10$ volume %[19] and experimental CNT data at $V_f > 20$ volume % is not available, we propose extending the linear fit in these regimes and using $V_f^{UB}(83.4,6)$ as a data point, which will most likely lead to significant errors at very high, and very low CNT volume fractions, where the data may not be linear, but should yield a more realistic slope for the range of available data (1.0 volume % $\leq V_f \leq 20$ volume %). The fitting equation takes the following form:

$$N(V_f) = a_2(V_f) + b_2 \tag{11}$$

Using this functional form, the data along with V_f^{UB} were fitted, and resulted in the following coefficients ($R^2 = 0.9761$): $a_2 = 2.511$, $b_2 = 3.932$. See Fig. 4 for a plot of the empirical N data, V_f^{UB}, and the linear fitting function. By combining Eqs. 9−11, and S2 from the ESI,† the N dependence of Γ_N can be removed, yielding the final form of the corrected average inter-CNT spacing (Γ) for the VACNT example:

$$\Gamma(D_{CNT}, V_f) = D_{CNT}\left(\zeta(V_f)\sqrt{\frac{0.9069}{V_f}} - 1\right) \tag{12}$$

$$\hookrightarrow \zeta(V_f) = 11.77(2.511(V_f) + 3.932)^{-3.042} + 0.9496$$

Since experimental data for average inter-CNT spacing for the entire physical range of CNT volume fraction (0 − 83 volume %) was not available, the accuracy of Eq. 12 for volume fractions above 20.0 volume % CNTs, and below 1.0 volume % CNTs is not known.

4.2 Application to VACNF Arrays

To test the applicability of the model to other nanowire systems of varying wire diameters, Eq. 12 was applied to a system of CNFs[38–42] with an average fiber diameter of 182 ± 56 nm.[42] But before Eq. 12 can be used to predict the average spacing for the designated CNF array,[42] the CNF volume fraction must be computed. Using the given fiber density of 2.2 $\frac{fibers}{\mu m^2}$ and the given

average fiber diameter of 182 nm.[42] the volume fraction is computed as 5.7 volume % CNFs, which yields a predicted average inter-CNF spacing of 625 nm. The reported (experimentally determined using HRSEM) average inter-CNF spacing for the system was 590 ± 200 nm,[42] meaning that the model over predicted the observed spacing by 5.9 %. Hexagonal and square packing predict an average inter-fiber spacing of 543 nm (-8.0%) and 632 nm (7.1%) respectively, suggesting that the continuous coordination model developed in this paper outperforms both of these common constant coordination models.

Using the evaluated CNF volume fraction, the reported average inter-CNF spacing, and assuming that the data provided was corrected for the depth information lost during the projection process (similar to Eq. S2 in the ESI†), N for the CNF system can be computed directly. The value of N for the reported CNF system, evaluated using Eq. 9, is 4.57, which exceeds the one calculated by Eq. 12 (4.16). The most likely reason why the predicted average inter-CNF spacing deviated from the one previously reported[42] is that the model assumes the CNFs in the array are collimated (their waviness is negligible). While the model could be better applied to VACNFs if average inter-CNF data was available for a variety of CNF volume fractions, the waviness of the CNFs is not easy to compensate for, and was intentionally not included in the theoretical derivation since nanowire waviness is not well understood, and cannot be modeled in a way that is universally applicable to all nanowire systems due to its strong dependence on synthesis and processing parameters.
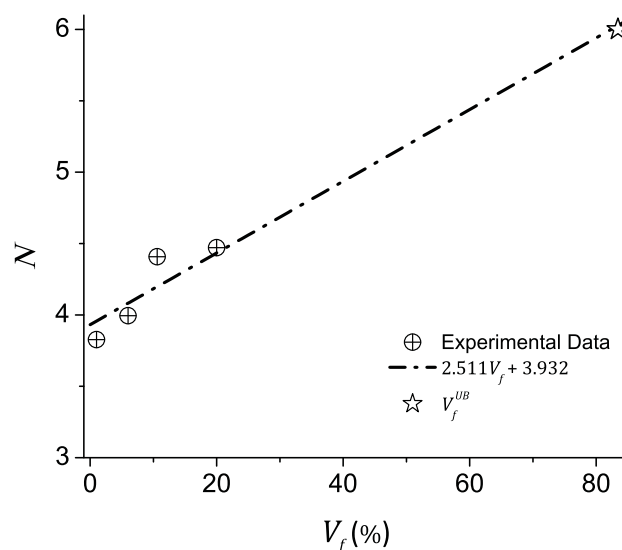
Fig. 4 Coordination number as a function of CNT volume fraction. The increase in coordination number is almost linear in between 1.0 and 20.0 volume %, as previously shown in a model developed for random packing of millimeter length scale disks in a plane by T.I. Quickenden and G.K. Tan.[19]

4.3 Waviness Correction

To transform the modeled nanowires from collimated to wavy nanowires, a correction term of the form $D\psi\omega$, where ω is defined as the waviness ratio (the ratio of the waviness amplitude and its wavelength) previously proposed for modeling wavy nanowire reinforcement in a polymer matrix composite using a sinusoidal wave equation,[47,48] and ψ is a scaling factor, may be included. Using a waviness correction factor, the general form of the average spacing equation can be written as follows:

$$\Gamma(D, V_f, \psi, \omega) = \Gamma(D, V_f) - D\psi\omega \qquad (13)$$

If the waviness correction is not included in the model, the model predicted average inter-wire spacing will always overestimate the observed average inter-wire spacings in real nanowire arrays, since the effective diameter of the wavy nanowires, D^e, will be larger than the nanowire diameter, D ($D^e = D$ in collimated nanowire arrays). An illustration of the distinction between wavy and collimated nanowires is provided in Fig. 5. Therefore, before the average inter-wire spacings for wavy nanowires can be accurately predicted, a model that precisely quantifies the waviness of wavy nanowires must be developed.
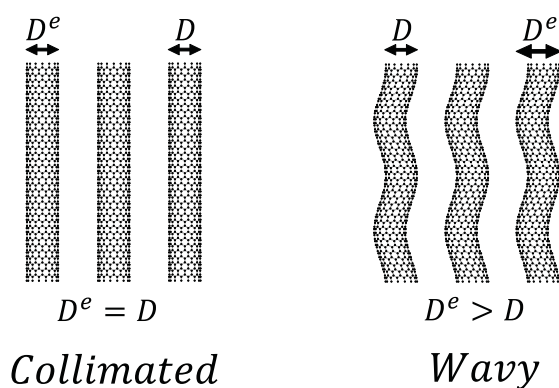
Fig. 5 Illustration of packing for both collimated and wavy nanowires. Since the model predicts average inter-wire spacings for collimated nanowires, where the nanowire diameter, D, is equal to the effective nanowire diameter, D^e, the figure demonstrates that the model generated predictions will overestimate the spacing in wavy nanowire systems, where $D^e > D$, until a model that precisely quantifies the waviness of wavy nanowires is developed.

5 Conclusions

In summary, a model that determines the average nanowire coordination number from the average nanowire inter-wire spacing, diameter and volume fraction is derived, and applied to 8 *nm* diameter VACNTs and 182 *nm* diameter VACNFs. By showing that the coordination number of nanowire arrays changes with the nanowire volume fraction, the model demonstrates that a continuous model of the coordination number is necessary,

and that the common assumptions of constant and negligible nanowire coordinations may not be adequate. To extend the range of validity of the continuous coordination model, average inter-wire spacing data for nanowire arrays with nanowire volume fractions below 1.0 volume % and above 20.0 volume % is required. To explore the validity of the model on smaller diameter nanowire arrays, future studies should extend this model to single walled CNTs (SWNTs), but since SWNTs have the added complexity of roping, there may be two levels of morphology that must be modeled. Also, a volume averaging method, such as small angle x-ray scattering (SAXS), is necessary for the collection of better average inter-wire spacing data, since: 1) the collection of representative inter-wire spacing data using microscopy requires the analysis of many micrographs; 2) the employed counting algorithm for determining the average inter-wire spacing from HRSEM micrographs was prone to counting errors due to a lack of surface feature depth information, and resolution to distinguish individual CNTs in bundles. Finally, to allow the accurate prediction of average inter-wire spacings for nanowire system, a model that precisely quantifies the waviness of wavy nanowires is required. Once a waviness model is developed, and data below 1.0 volume % and above 20.0 volume % is available, this model could be used to accurately predict the average inter-wire spacing of many aligned nanowire systems at a broad range of nanowire volume fractions, a capability that will greatly benefit nano science.

References

1   A. Bezryadin, C. N. Lau, and M. Tinkham, Nature **404**, 971 (2000).

2   J. E. Mooij and Y. Nazarov, Nat. Phys. **2**, 169 (2006).

3   J. Wang, M. Singh, M. Tian, N. Kumar, B. Liu, C. Shi, J. K. Jain, N. Samarth, T. E. Mallouk, and M. H. W. Chan, Nat. Phys. **6**, 389 (2010).

4   K. Xu and J. R. Heath, Nano Lett. **8**, 3845 (2008).

5   S. Shen, A. Henry, J. Tong, R. Zheng, and G. Chen, Nat. Nanotechnol. **5**, 251 (2010).

6   Y. Zhang, M. S. Dresselhaus, Y. Shi, Z. Ren, and G. Chen, Nano Lett. **11**, 1166 (2011).

7   B. Wu, A. Heidelberg, and J. J. Boland, Nat. Mater. **4**, 525 (2005).

8   C. Q. Chen, Y. Shi, Y. S. Zhang, J. Zhu, and Y. J. Yan, Phys. Rev. Lett. **96**, 075505 (2006).

9   B. Wen, J. E. Sader, and J. J. Boland, Phys. Rev. Lett. **101**, 175502 (2008).

10 H. Yan, H. S. Choe, S. Nam, Y. Hu, S. Das, J. F. Klemic, J. C. Ellenbogen, and C. M. Lieber, Nature **470**, 240 (2011).

11 Y. Cui, Q. Wei, H. Park, and C. M. Lieber, Science **293**, 1289 (2001).

12 R. Vasita and D. S. Katti, Int. J. Nanomedicine **1**, 15 (2006).

13 C. K. Chan, H. Peng, G. Liu, K. McIlwrath, X. F. Zhang, R. A. Huggins, and Y. Cui, Nat. Nanotechnol.. **3**, 31 (2008).

14 C. A. Huber, T. E. Huber, M. Sadoqi, J. A. Lubin, S. Manalis, and C. B. Prater, Science **263**, 800 (1994).

15 D. N. Futaba, K. Hata, T. Yamada, T. Hiraoka, Y. Hayamizu, Y. Kakudate, O. Tanaike, H. Hatori, M. Yumura, and S. Iijima, Nat. Mater. **5**, 987 (2006).

16 L. Liu, W. Ma, and Z. Zhang, Small **7**, 1504 (2011).

17 A. M. Marconnet, N. Yamamoto, M. A. Panzer, B. L. Wardle, and K. E. Goodson, ACS Nano **5**, 4818 (2011).

18 H. Kausch, D. Fesko, and N. Tschoegl, J. Colloid Interface Sci. **37**, 603 (1971).

19 T. I. Quickenden and G. K. Tan, J. Colloid Interface Sci. **48**, 382 (1974).

20 D. Sutherland, J. Colloid Interface Sci. **60**, 96 (1977).

21 E. W. Wong, P. E. Sheehan, and C. M. Lieber, Science **277**, 1971 (1997).

22 D. A. Walters, L. M. Ericson, M. J. Casavant, J. Liu, D. T. Colbert, K. A. Smith, and R. E. Smalley, Appl. Phys. Lett. **74**, 3803 (1999).

23 M.-F. Yu, B. S. Files, S. Arepalli, and R. S. Ruoff, Phys. Rev. Lett. **84**, 5552 (2000).

24 S. Frank, P. Poncharal, Z. L. Wang, and W. A. d. Heer, Science **280**, 1744 (1998).

25 W. Liang, M. Bockrath, D. Bozovic, J. H. Hafner, M. Tinkham, and H. Park, Nature **411**, 665 (2001).

26 R. H. Baughman, A. A. Zakhidov, and W. A. de Heer, Science **297**, 787 (2002).

27 P. Kim, L. Shi, A. Majumdar, and P. L. McEuen, Phys. Rev. Lett. **87**, 215502 (2001).

28 M. Kociak, A. Y. Kasumov, S. Guron, B. Reulet, I. I. Khodos, Y. B. Gorbatov, V. T. Volkov, L. Vaccarini, and H. Bouchiat, Phys. Rev. Lett. **86**, 2416 (2001).

29 Z. K. Tang, L. Zhang, N. Wang, X. X. Zhang, G. H. Wen, G. D. Li, J. N. Wang, C. T. Chan, and P. Sheng, Science **292**, 2462 (2001).

30 Z. F. Ren, Z. P. Huang, J. W. Xu, J. H. Wang, P. Bush, M. P. Siegal, and P. N. Provencio, Science **282**, 1105 (1998).

31 S. Fan, M. G. Chapline, N. R. Franklin, T. W. Tombler, A. M. Cassell, and H. Dai, Science **283**, 512 (1999).

32 Y. Murakami, S. Chiashi, Y. Miyauchi, M. Hu, M. Ogura, T. Okubo, and S. Maruyama, Chem. Phys. Lett. **385**, 298 (2004).

33 K. Hata, D. N. Futaba, K. Mizuno, T. Namai, M. Yumura, and S. Iijima, Science **306**, 1362 (2004).

34 F. Fachin, G. Chen, M. Toner, and B. Wardle, *Microelectromechanical Systems, Journal of*, J. Microelectromech. Syst. **20**, 1428 (2011).

35 B. L. Wardle, D. S. Saito, E. J. García, A. J. Hart, R. Guzmán de Villoria, and E. A. Verploegen, Adv. Mater. **20**, 2707 (2008).

36 S. Vaddiraju, H. Cebeci, K. K. Gleason, and B. L. Wardle, ACS Appl. Mater. Interfaces **1**, 2565 (2009).

37 E. J. Garcia, B. L. Wardle, A. John Hart, and N. Yamamoto, Compos. Sci. Technol. **68**, 2034 (2008).

38 V. I. Merkulov, D. H. Lowndes, Y. Y. Wei, G. Eres, and E. Voelkl, Appl. Phys. Lett. **76**, 3555 (2000).

39 V. I. Merkulov, A. V. Melechko, M. A. Guillorn, D. H. Lowndes, and M. L. Simpson, Appl. Phys. Lett. **79**, 2970 (2001).

40 V. I. Merkulov, M. A. Guillorn, D. H. Lowndes, M. L. Simpson, and E. Voelkl, Appl. Phys. Lett. **79**, 1178 (2001).

41 L. Zhang, A. V. Melechko, V. I. Merkulov, M. A. Guillorn, M. L. Simpson, D. H. Lowndes, and M. J. Doktycz, Appl. Phys. Lett. **81**, 135 (2002).

42 J. D. Fowlkes, B. L. Fletcher, E. D. Hullander, K. L. Klein, D. K. Hensley, A. V. Melechko, M. L. Simpson, and M. J. Doktycz, Nanotechnology **16**, 3101 (2005).

43 C. F. Gauss, Göttingsche Gelehrte Anzeigen (1831).

44 S. Kärkkäinen, A. Miettinen, T. Turpeinen, J. Nyblom, P. Pötschke, and J. Timonen, Image Anal. Stereol. **31**, 17 (2012).

45 S. Pegel, P. Pötschke, T. Villmow, D. Stoyan, and G. Heinrich, Polymer **50**, 2123 (2009).

46 S. Amelinckx, *Handbook of Microscopy (VCH) – Series* (VCH, 1997).

47 H. Cebeci, R. Guzmán de Villoria, A. J. Hart, and B. L. Wardle, Compos. Sci. Technol. **69**, 2649 (2009).

48 F. T. Fisher, R. D. Bradshaw, and L. C. Brinson, Appl. Phys. Lett. **80**, 4647 (2002).

Electronic Supplementary Information: Coordination Number Model to Quantify Packing Morphology of Aligned Nanowire Arrays

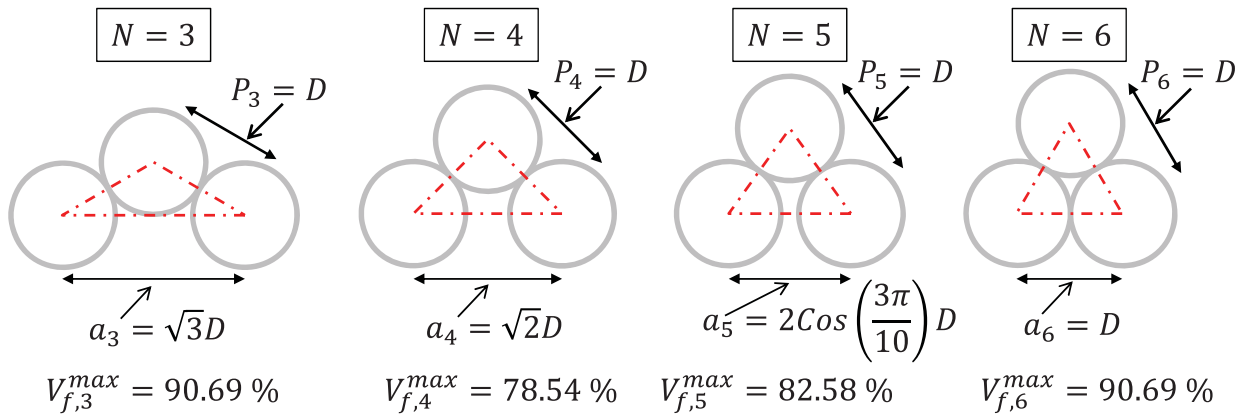**Itai Y. Stein,[*][a][§] and Brian L. Wardle[b][§]**

[a] Department of Mechanical Engineering, Massachusetts Institute of Technology, 77 Massachusetts Ave, Cambridge, MA 02139, USA. E-mail: iys@mit.edu
[b] Department of Aeronautics and Astronautics, Massachusetts Institute of Technology, 77 Massachusetts Ave, Cambridge, MA 02139, USA.
§ NECSTlab

Table S1 Triangle areas, and volume fractions for all coordinations.

N	$A_{\triangle,\,N}(P_N)$	$V_{f,\,N}(D,P_N)$
3	$\frac{\sqrt{3}}{4}P_N^2$	$\frac{\sqrt{3}\pi}{6}\left(\frac{D}{P_N}\right)^2$
4	$\frac{1}{4}P_N^2$	$\frac{\pi}{4}\left(\frac{D}{P_N}\right)^2$
5	$cos\left(\frac{3\pi}{10}\right)sin\left(\frac{3\pi}{10}\right)P_N^2$	$\frac{\pi}{8cos\left(\frac{3\pi}{10}\right)sin\left(\frac{3\pi}{10}\right)}\left(\frac{D}{P_N}\right)^2$
6	$\frac{\sqrt{3}}{4}P_N^2$	$\frac{\sqrt{3}\pi}{6}\left(\frac{D}{P_N}\right)^2$

$$N=3 \qquad N=4 \qquad N=5 \qquad N=6$$

$$P_3=D \qquad P_4=D \qquad P_5=D \qquad P_6=D$$

$$a_3=\sqrt{3}D \qquad a_4=\sqrt{2}D \qquad a_5=2Cos\left(\frac{3\pi}{10}\right)D \qquad a_6=D$$

$$V_{f,3}^{max}=90.69\,\% \qquad V_{f,4}^{max}=78.54\,\% \qquad V_{f,5}^{max}=82.58\,\% \qquad V_{f,6}^{max}=90.69\,\%$$
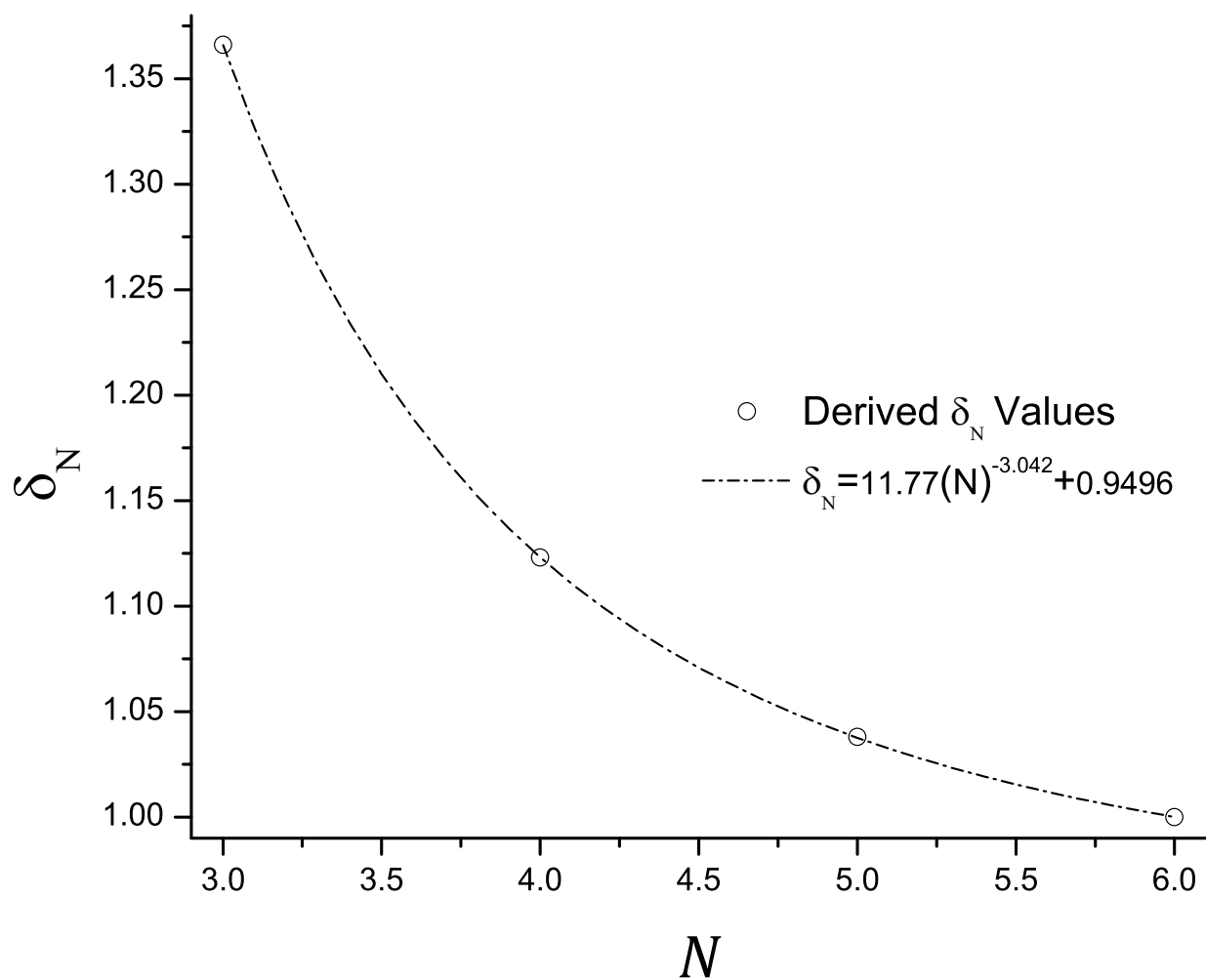
Fig. S1 Illustration of component triangles for each coordination at the maximum theoretical volume fractions (wire walls are touching). Since the unit cell inter-wire spacing, S_N, is zero in this case, P_N, is equal to the wire diameter, D, in all coordinations.

1

Table S2 Lattice constant, Chi parameter, and average inter-wire spacing for all coordinations.

N	$a_N(D,V_f)$	χ_N	$\Gamma_N(D,V_f)$
3	$\sqrt{3}D\left(\sqrt{\frac{V_{f,3}^{max}}{V_f}}\right)$	$\sqrt{3}$	$D\left(\left(\frac{\sqrt{3}+1}{2}\right)\left(\sqrt{\frac{V_{f,3}^{max}}{V_f}}\right)-1\right)$
4	$\sqrt{2}D\left(\sqrt{\frac{V_{f,4}^{max}}{V_f}}\right)$	$\sqrt{2}$	$D\left(\left(\frac{\sqrt{2}+1}{2}\right)\left(\sqrt{\frac{V_{f,4}^{max}}{V_f}}\right)-1\right)$
5	$2cos\left(\frac{3\pi}{10}\right)D\left(\sqrt{\frac{V_{f,3}^{max}}{V_f}}\right)$	$2cos\left(\frac{3\pi}{10}\right)$	$D\left(\left(\frac{2cos\left(\frac{3\pi}{10}\right)+1}{2}\right)\left(\sqrt{\frac{V_{f,3}^{max}}{V_f}}\right)-1\right)$
6	$D\left(\sqrt{\frac{V_{f,6}^{max}}{V_f}}\right)$	1	$D\left(\sqrt{\frac{V_{f,6}^{max}}{V_f}}-1\right)$

Table S3 Deviation factor for all coordinations.

| N	$\delta_N(D,V_f)$
3	$\left(\frac{\sqrt{3}+1}{2}\right)$
4	$\sqrt{\frac{\sqrt{3}}{2}}\left(\frac{\sqrt{2}+1}{2}\right)$
5	$\sqrt{\frac{\sqrt{3}}{4cos\left(\frac{3\pi}{10}\right)sin\left(\frac{3\pi}{10}\right)}}\left(\frac{2cos\left(\frac{3\pi}{10}\right)+1}{2}\right)$
6	1

Fig. S2 Plot of the deviation factor from hexagonal packing, δ_N, as a function of nanowire coordination number, N, using the functional form given in Eq. 8.

Final form of the average inter-wire spacing equation for $3 \leq N \leq 6$:

$$\Gamma_N(D, V_f) = D\left((11.77(N)^{-3.042} + 0.9496)\sqrt{\frac{0.9069}{V_f}} - 1\right) \tag{S1}$$

Correction equation for average inter-wire spacings extracted from HRSEM micrographs:

$$\Gamma_N(D, V_f) = \frac{\Gamma_N^{SEM}}{Cos\left(ArcTan\left(\frac{\ell_e^{SE}}{\Gamma_N^{SEM}}\right)\right)} \tag{S2}$$
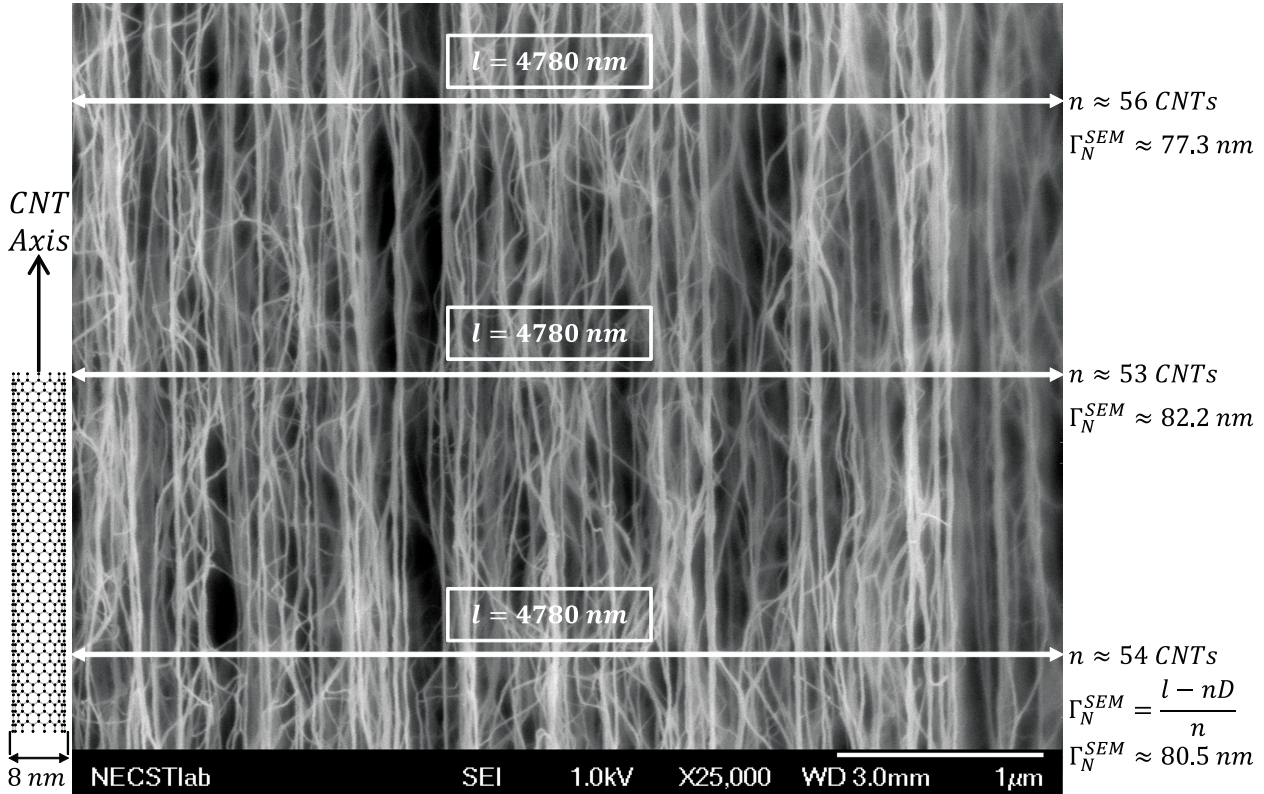
Fig. S3 HRSEM micrograph for a 1.0 volume % CNT forest with lines drawn perpendicular to the CNT primary axis. The average inter-CNT spacing in the forest was then determined by counting only the bright in-focus CNTs underneath each line.